Applied Physics A (2023) 129:143
https://doi.org/10.1007/s00339-023-06428-0

Applied Physics A
Materials Science & Processing

S.I. : 50TH ANNIVERSARY OF APPLIED PHYSICS

Simulation and characterization of $CH_3NH_3SnI_3$-based perovskite solar cells with different Cu-based hole transporting layers

Shayesteh Imani[1] · Seyedeh Mozhgan Seyed-Talebi[1,2] · Javad Beheshtian[1] · Eric Wei Guang Diau[2,3]

Received: 1 November 2022 / Accepted: 15 January 2023

Abstract

Perovskite solar cells (PSCs) are extremely attractive due to having low processing cost, easy solution processing, and excellent light-harvesting characteristics along with their recent rapid development. PCSs are made of different layers that affect the performance of the devices. Hole transporting layers (HTLs) are one of the layers that have a significant effect on conducting the carriers and enhancing the efficiency of PSCs. In the present study, the results of computational simulation using the SCAPS-1D software for devices made of the $MASnI_3$ perovskite light absorber and different inorganic Cu-based HTLs, such as CuSCN, Cu_2O, CuO, CuI, $SrCu_2O_2$, and $CuSbS_2$, are presented, in comparison with the standard contain Spiro-OMeTAD-based device. The modification effects of the perovskite absorber layer thickness, total defect density (N_t), the band gap of the absorber, the thickness of HTLs, and the operational temperature on the characteristic photovoltaic parameters were analyzed. The highest power conversion efficiency (PCE) was obtained to be 32.13%, with a fill factor (FF) of 87.08%, open-circuit voltage (V_{OC}) of 1.07 V, and short-circuit current density (J_{SC}) of 34.35 mA cm^{-2}, for CuI as an efficient HTL in comparison with the other HTLs. We believe that the current theoretical results provided profound insights into the development of new high-performance, low-cost, and lead-free PSCs with Cu-based HTLs.

Keywords Cu-based HTL · Hole transporting layer · $MASnI_3$ · Perovskite solar cell · SCAPS-1D software

1 Introduction

Considering the fact of rapidly depleted fossil fuels and the environmental pollutions caused by them, finding clean and renewable sources of energy seems to be an urgent task to proceed. According to the research studies on solar energy, the most abundant and cheapest available source of renewable energy is electricity generated by solar irradiation, and it is the best option to replace fossil fuels in future [1–3]. Photovoltaic cells play a major role in future energy systems. Scientists have organized different kinds of solar cell. Among them, perovskite solar cells (PSCs) have attracted much attention in the solar cell research field. PSCs have some features that make them more significant in comparison with other kinds of solar cells, including unique optoelectronic features, high absorption ability, low-cost processing, high performance, ease of preparation, and great charge carrier diffusion length [4–10]. First time in 2009, Kojima et al. achieved an efficiency of 3.8% for PSCs [11]. The performance of lead-based PSCs had a sharp increase and in 2021, Min et al. succeeded to access efficiency of 25.8% [12]. The formation of an interlayer between a tin dioxide (SnO_2) layer as ETL and a halide perovskite light-absorbing layer, made by coupling Cl-bonded SnO_2 with a Cl-containing perovskite is reported [13]. By organizing the chemical bath deposition of SnO_2 as ETL, Yoo et al. could achieve a PCE of 25.2% in lead-based PSCs with great film coverage, thickness, and composition. They also decoupled the passivation between the bulk and the interface, which leads to improved morphological features and minimizes the band-gap penalty [13]. Both of these results are related to experimental studies for lead-based PSCs. In theoretical studies, the performance may have higher values than the

✉ Eric Wei Guang Diau
diau@nycu.edu.tw

[1] Department of Chemistry, Shahid Rajaee Teacher Training University, Tehran, Iran

[2] Department of Applied Chemistry and Institute of Molecular Science, National Yang Ming Chiao Tung University, 1001 Ta-Hseuh Rd., Hsinchu 300093, Taiwan

[3] Center for Emergent Functional Matter Science, National Yang Ming Chiao Tung University, 1001 Ta-Hseuh Rd., Hsinchu 300093, Taiwan

Published online: 24 January 2023

Shockley–Queisser limit. Hosseini et al., in their research tried to show a new insight on the perovskite solar cells via simulation in non-ideal conditions using the SCAPS-1D software. They confirmed that the theoretical studies using the non-ideal model would help researchers to validate experimental data with the simulated results, and compare the results of simulation with experimental data [14]. Mushtaq et al. reported modification of the thickness and defect density of the absorber layer, the film thickness and doping concentration of all ETLs and HTLs, acceptor and donor doping charge concentration of the absorption layer, back contact work function, interface defect density of the HTL/perovskite layer, and perovskite layer/ETL, series and shunt resistances using the SCAPS-1D software to achieve a PCE of 34.52% and a FF of 88.30% for optimized device [15]. Although the results of the simulation in present research are higher than the expected experimental outcome, the comparative results will give helpful insights to experimentalists for utilizing Cu-based HTLs in their devices to attain higher device performance.

Organic–inorganic hybrid perovskites can be expressed as ABX_3, in which A is a monovalent inorganic or organic cation, such as methylammonium (MA), formamidinium (FA), or cesium (Cs^+); B is a divalent cation, such as Pb^{2+}, Sn^{2+}, and Ge^{2+}; X is a monovalent anion, such as Cl^-, Br^-, and I^- [16]. In the early years, researchers developed only lead (Pb) for PSCs. However, Pb is not environmentally friendly and has deleterious effects on humans and the environment [17–19]. Therefore, scientists have utilized some other cations to replace Pb. The applicable cations for the formation of perovskite structures are Bi, Sb, Sn, Ge, and Cu [20]. In 2019, Weijun et al., summarized the present status and future prospects for lead-free perovskite materials and their devices, indicating that Sn is the best replacement among all of the other candidates [21]. Sn and Pb are in a similar periodic group, and they have the same valence electronic configuration (ns^2np^2). Furthermore, Sn-based perovskites have features that are comparable to lead-based perovskites, such as long carrier lifetimes, doping densities, long diffusion lengths, smaller optical band gaps, and high electron and hole mobilities, $MASnI_3$ has an exceptionally low bimolecular constant to mobility ratio same as $MAPbI_3$. Therefore, Sn is a good alternative for Pb to replace in the Pb-based perovskite layers [22]. Numerous studies have been conducted for enhancing the quality of tin-based perovskite layers, and there is an increase in the utilization of tin halide-based materials as substitutes for toxic lead halide-based absorbers [23–26]. In 2021, Bhattarai et al. performed a comprehensive simulation of organic/inorganic perovskite-based photovoltaic solar cells under the preconditioned illumination of AM1.5 for distinct device structures. The simulated structures for both devices validate that lead-free ($MASnI_3$) PSC has a more significant performance in comparison with a lead-based PSC with many extensive benefits of eco-friendliness and stability factors because it extremely increases the PCE than the earlier reported amount of Noel et al., [27, 28]. It is worth mentioning that the effect of other layers of tin-based PSCs on device performance was not investigated.

In 2020, Karimi et al. studied the performance of PSCs via the Analysis of Microelectronic and Photonic Structures (AMPS) and the Solar Cell Capacitance Simulator (SCAPS-1D) simulation software programs. They reported the importance of ETL and HTL roles on the performance of PSCs. Both of the ETL and HTL transfer the charge ions from the absorber layer to the electrodes and act as separation layers between them [29]. HTLs are an important part of PSCs, and they have significant effects on the cost, performance, and stability of PSCs. In comparison with the organic layers, some inorganic HTLs have high transparency, favorable and tunable energy alignment with the perovskite layer, higher stability against moisture, light, and heat, higher hole mobility, and suitable hole collection with cost-effective processes [30]. The major concern with respect to the standard solar cell with Spiro- OmeTAD as most commonly used organic HTL is its expensive and complex manufacturing process. Furthermore, the long-term stability and its poor sustainability are another important issues [31]. Hence, exploitation of Spiro-OMeTAD as an organic HTL can obstruct the commercialization of the perovskite solar cells. It is necessary to replace the costly and unstable HTM with a stable and cheaper HTM with high mobility. The inorganic HTLs are also considered desirable barrier layers for protecting the perovskite layer. The wide band gap of inorganic HTLs leads to high transition, deep valence band (VB) position, low conduction band (CB) edges, and high V_{OC} to block the effective transportation of electrons to anodes [32]. In comparison to the organic HTMs, inorganic HTMs illustrate the benefits of great hole mobility, good chemical stability, wide energy gap, and low cost. The inorganic HTMs including Ni-based, Cu-based, V_2O_5, and MoO_3 have been utilized in lead-based PSCs as hopeful next-generation of HTMs [33]. Among inorganic HTMs, Cu-based inorganic HTMs, such as CuI, CuSCN, Cu_2O, and CuO, and their derivatives, are reported in lead-based PSCs. In addition, Cu-based inorganic HTMs have some unique merits, including their scalable processing ability, low temperature, rich variety, and adjustable energy levels. These properties cause Cu-based inorganic semiconductors to become a promising candidate to use as the HTMs for future commercial PSCs [33–35].

The Cu derivatives HTLs can achieve PCE comparable with standard organic HTMs that have been integrated so far. Having higher stability at a minimized expense, the well-tuned energy levels which can conform to all of the different constitutions of the perovskite layer made them suitable for using in solar cell devices [34]. Copper iodide (CuI) is a wide band-gap semiconductor (3.1 eV) with three crystalline

phases a, b, and g. Among these crystalline phases, g-phase CuI acts as a p-type semiconductor. CuI has also attracted great attention due to its high hole conductivity, large band-gap, solution processability, and low cost. [36]. The CuSCN has favorable properties as HTM for PSC, such as high hole mobility, wide band-gap (3.8 eV), and good thermal stability [36]. Copper oxide (CuO) and cuprous oxide (Cu_2O) are well-known as p-type semiconductors due to the natural abundance of copper [36]. Low-lying V_B of CuO and Cu_2O well matches with perovskite layer, and the energy loss minimizes when being used as HTM in PSCs. Cu_2O exhibits high hole mobility (~90 cm^2V^{-1} s^{-1}) due to its tetrahedral coordination leading to larger dispersion of the V_B and deep-lying V_B owing to ~ 2 eV band-gap [36]. Inorganic p-type transparent conductive oxide such as $SrCu_2O_2$ has been found to be good candidate to apply as a hole conductor in solar cells with appropriate valance and conduction band position [37]. The planar Sn-based Perovskite Solar Cell Design with copper antimony sulfide ($CuSbS_2$) as the Hole Transport Layer (HTL) is because of its ingrained properties like large open-circuit voltage and high abundance in comparison with Spiro OMe-TAD, which has lack of stability and is expensive [38]. Utilizing CuI as an inorganic HTM in $CH_3NH_3SnI_3$-based PSC, the excellent improvement in Fill Factor (FF) of 82.45% and Power Conversion Efficiency (PCE) of 36.18% reported [38]. In 2021, Matondo et al. gave an outline of the organization of inorganic copper-based HTMs in normal and inverted PSC structures and focused on the Cu-based HTMs' potential to overcome the issues of using organic HTMs in PSCs, to increase the interest of using these materials for the improvement in the performance of the PSC devices [39]. In 2021, Ye et al. summarized systematically the research improvement in new materials and the control of photoelectric features of Cu-based inorganic HTMs. They discussed various processing methods and progress in interfacial engineering of the Cu-based HTLs and the challenges and future developments of Cu-based inorganic HTMs. They concluded that Cu-based inorganic HTMs certainly will take their role in PSCs with the advantages of low cost, great stability, and wide applications [40]. Omarova et al. in a study illustrated the effect of interface defects at the interfaces of $TiO_2/CH_3NH_3SnI_3$ and $CH_3NH_3SnI_3$/HTL across the same defect densities range. Their simulations focus on the effect of bulk defects on the absorbing layer, temperature, interfacial defects, and perovskite thickness on the device performance. In addition, they found that the PSC has the most efficient at 300 K, in the absence of ionic contribution [41]. Shyma et al., have done a simulation of a planar hetero-junction Tin-based ($CH_3NH_3SnI_3$) perovskite solar cell by SCAPS-1D software [42]. Device parameters, such as the thickness and the defect density of the absorber layer, temperature, etc., were investigated. Enhancing the thickness of the perovskite induced the J_{sc} amount. As the defect density of the absorber layer is enhanced, all device parameters decrease drastically. The temperature decreased the performance of the device. This may be because of more recombination speed and subsequent enhancement in the series resistance. The rise in the environment temperature caused decrease the performance of devices [42]. SCAPS-1D program has been organized to design the solar cell and analyze its performance. Researchers at the department of ELIS of the University of Gent, Belgium have designed the numerical simulation tool SCAPS-1D [43]. In the present study, inorganic Cu-based p-type semiconductors are used as HTMs in PSCs because of their unique advantages of low cost, great variety, high hole mobility, good stability, low-temperature processing, adjustable energy levels, and capability of scalable processing. The Cu^+-based oxychalcogenides, chalcogenides, and halides have high p-type conductivity compared to Cu-based oxides. Since the p orbitals of halogens (Cl, Br, and I) and chalcogenides (Se, S, O, and Te) are more delocalized in comparison with oxygen 2p orbitals, the halogens/chalcogens make more hybridization between Cu $3d^{10}$ and chalcogenides/halogens p orbitals, which leads to a higher dispersive VB and more p-type conductivity [44]. The parameters of other layers are constant. The influence of input parameters has been examined by simulation using SCAPS-1D software. The present research proposes a tin halide PSC (TH-PSC) designed with Glass/TCO/$TiO_2/CH_3NH_3SnI_3$/HTL/Au structure as a normal type device and the effect of thickness, defect density, the band gap of perovskite layer, the thickness of HTL, and temperatures have been investigated.

2 Methodology

The SCAPS-1D is a solar cell simulation software program. In this study, Solar Cell Capacitance Simulator-one Dimension (SCAPS-1D) version 3.3.08 was used due to its advantages, such as modeling in bright and dark status, control and facility of using, and the ability to make a seven various layer hetero-structure structure using SCAPS [43, 45]. The modeling in SCAPS-1D is based on the solution of Poisson's equation and continuity equations of holes and electrons. This program numerically solves these equations for the electrostatic potentials of electron and hole concentrations as a function of positions x [45].

$$\frac{d}{dx}\left(\varepsilon(x)\frac{d\Psi}{dx}\right) = q[p(x) - n(x)N_D^+(x) - N_A^-(x) + Pt(x) - nt(x)] \quad (1)$$

$$\frac{1}{j}\frac{dJ_P}{dx} + RP(X) - G(X) = 0 \quad (2)$$

$$-\frac{1}{j}\frac{dJ_n}{dx} + Rn(X) - G(X) = 0 \quad (3)$$

Here, ε signifies the permittivity, q signifies an electron charge, ψ signifies the electrostatic potential, n signifies the concentrations of electrons, p signifies the concentrations of free holes, n_t signifies the trapped electron, P_t signifies the trapped hole, N_D^+ signifies the ionized donor-like doping, and N_A^- signifies the concentrations of ionized acceptor-like doping. $R_n(x)$ signifies the recombination rate of electrons and $R_p(x)$ signifies that of holes, and $G(x)$ signifies the generation rate. J_n signifies the current density of the electrons and J_p signifies the current density of holes [46]. Input simulation parameters of the simulated layers are extracted from previous experimental or theoretical publications. The input simulation parameters of the proposed layers are presented in Table 1.

2.1 Simulated device structures

The normal type structure of simulated devices is formed from glass/TCO/ETL/ perovskite absorber/HTL/Au. As shown in Fig. 1, in this structure, the Cu-based layers, such as CuSCN, Cu_2O, CuO, CuI, $SrCu_2O_2$, $CuSbS_2$, and Spiro-OMeTAD, are utilized as HTLs. $CH_3NH_3SnI_3$ is a perovskite absorber layer, TiO_2 is an ETL, and TCO is the transparent conductive oxide substrate. Glass is under the TCO and light falls on the glass side [52, 53]. Figure 1 demonstrates the schematic diagram of a planar n-i-p photovoltaic solar cell, which is simulated through the SCAPS-1D 3.3.08 for solving Poisson's equation and continuity equations for the simulation of the solar cell [45]. An AM1.5G spectrum is employed for illuminating the device (1000 W m^{-2}; $T = 300$ K).

The location of the energy levels of the CuSCN, Cu_2O, CuO, CuI, $SrCu_2O_2$, $CuSbS_2$, and Spiro-OMeTAD HTLs is shown in Fig. 2.

According to the plotted schematic diagram in Fig. 2, and the listed valence band offsets (VBOs) for CuSCN, Cu_2O, CuO, CuI, $SrCu_2O_2$, $CuSbS_2$, and Spiro-OMeTAD in Table 2 are 0.08, − 0.1, − 0.1, 0.03, 0.03, 0.31 and − 0.17 eV, respectively. Whenever VBO is negative, there is no obstacle for photo-generated holes to flow toward the HTLs; therefore J_{sc} becomes constant [54]. The positive value of the VBO makes a barrier that prohibits photo-generated holes from the perovskite to the HTLs. However, a large negative value of VBO results in an increase in the concentration of holes at the interface of the perovskite and the HTL, which leads to a recombination process at the interface of the absorber and the HTL. Hence, to have a good efficiency of the device, layers with a proper VBO should be considered to improve band alignment [15]. In the present study, VBO for Cu_2O, CuO, and Spiro-OMeTAD is negative, so hole transport would be easier

Table 1 Input parameters of simulated layers of PSC devices by SCAPS-1D software

Materials	E_g (eV)	N_t (1/cm^3)	N_D (cm^{-3})	N_A (cm^{-3})	ε	μ_p(cm^{2}v^{-1} s^{-1})	μ_n (cm^{2}v^{-1} s^{-1})	N_v (cm^{-3})	N_C (cm^{-3})	χ (eV)	E_g (eV)	Thickness (μm)
TCO	3.5	0.5	$2.0\times10^{+16}$	0	9	10	20	$1.8\times10^{+19}$	$2.2\times10^{+18}$	4.0	3.5	0.5
TiO_2	3.2 [48]	0.03 [46]	$1.0\times10^{+16}$	0	9	10	20	$1.8\times10^{+19}$ [50]	$2.0\times10^{+18}$ [50]	4.26 [47]	3.2 [48]	0.03 [47]
$CH_3NH_3SnI_3$	1.3 [47]	0.75	0.0	$3.2\times10^{+1}$	8.2 [51]	1.6 [27]	1.6 [27]	$1.0\times10^{+18}$	$1.0\times10^{+18}$	4.17 [47]	1.3 [47]	0.75
CuSCN	3.4	0.35	0.0	$1.0\times10^{+18}$	10	1.0	$2.0\times10^{+4}$	$1.8\times10^{+19}$	$2.5\times10^{+18}$	2.1	3.4	0.35
Cu_2O	2.17 [49]	0.05	0.0	$1.0\times10^{+20}$	7.5	$8.0\times10^{+1}$	$2.0\times10^{+1}$	$1.8\times10^{+19}$	$2.0\times10^{+18}$	3.2 [50]	2.17 [49]	0.05
CuO	1.3	0.15	0.0	$1.0\times10^{+18}$	18.1	1.0×10^{-1}	1.0×10^{-1}	$1.0\times10^{+19}$	$2.2\times10^{+18}$	4.07	1.3	0.15
CuI	3.4	0.05	0.0	$1.0\times10^{+20}$	10	$2.0\times10^{+4}$	$2.0\times10^{+4}$	$1.8\times10^{+19}$	$2.5\times10^{+18}$	2.1	3.4	0.05
$SrCu_2O_2$	3.3	0.1	0.0	$6.1\times10^{+17}$	9.77 [45]	4.6×10^{-1}	1.0×10^{-1}	$1.8\times10^{+19}$	$2.5\times10^{+18}$	2.2	3.3	0.1
$CuSbS_2$	1.58	0.4	0.0	$1.38\times10^{+18}$	14.6	$4.9\times10^{+9}$	$4.9\times10^{+1}$	$1.0\times10^{+19}$	$2.5\times10^{+18}$	4.2	1.58	0.4
Spiro-OMeTAD	3.2 [47]	0.05	0.0	$1.0\times10^{+20}$	3	$2.0\times10^{+4}$	$2.0\times10^{+}$	$1.0\times10^{+19}$	$2.0\times10^{+18}$	2.1 [47]	3.2 [47]	0.05

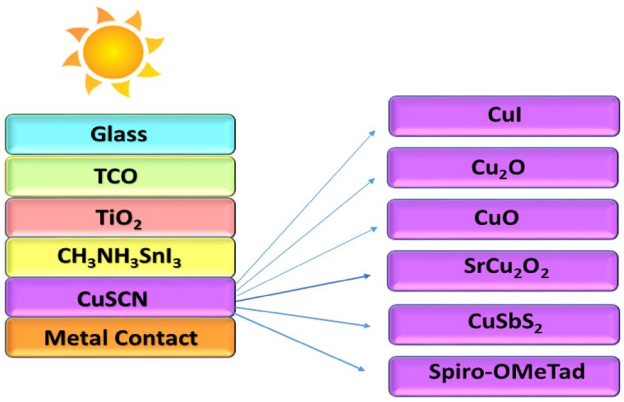

Fig. 1 The planar structure of the PSC

for these layers. Spiro-OMeTAD has larger negative VBO which leads to an increase in the recombination process at the interface of the absorber and the HTL and reducing the Voc value.

Table 2 The various HTLs valence band offset (VBO) with perovskite absorber

HTL	VBO (eV)
Cu_2O	− 0.1
CuI	+0.03
$SrCu_2O_2$	+0.03
CuO	− 0.1
$CuSbS_2$	+0.31
CuSCN	+0.08
Spiro-OMeTAD	− 0.17

Table 3 The photovoltaic parameters simulated using SCAPS-1D software for varied hole-transfer layer (HTL)

HTL	J_{SC} (mA/cm^2)	V_{OC} (V)	FF (%)	PCE (%)
Cu_2O	34.33	0.97	85.23	28.33
CuI	34.35	1.07	87.08	32.13
$SrCu_2O_2$	34.33	0.96	84.90	27.94
CuO	34.42	0.93	83.61	26.63
$CuSbS_2$	34.39	1.06	78.48	28.73
CuSCN	34.34	0.97	85.17	28.32
Spiro-OMeTAD	34.32	0.93	83.88	26.77

3 Results and discussion

Utilizing HTL in the structure of PSCs impacts on the performance of devices by blocking electrons, facilitating holes moving from the absorber layer to the back contact layer, and decreasing the recombination rate of electron–hole. The HTM possess positive charge carrier mobility, proper band-gap, optimized doping charge concentration, and optimized thickness [15]. In theoretical studies because of ideal situations, the photovoltaic parameters may be calculated to be higher than the real values. The simulated results of present research calculated by varying the HTL material and keeping fixed the ETL and perovskite layers are summarized in Table 3. The photovoltaic parameters of different simulated devices were obtained by running the SCAPS-1D software.

3.1 Current density–voltage (J–V) characterization

The current density–voltage curves of our simulated devices using the input parameters provided in Table 3 are shown in Fig. 3. The fill factor (FF) explains the square form of the current–voltage (*J–V*) curve and the rate of photo-generated carriers in a photovoltaic device. When the *J–V* curve is a rectangle, the ideal value for the FF is 100%. In case there is no match between the mobility of electrons and holes, the carriers with lower mobility will be accumulated in the solar cell. This will cause an additional electric field in the PSC,

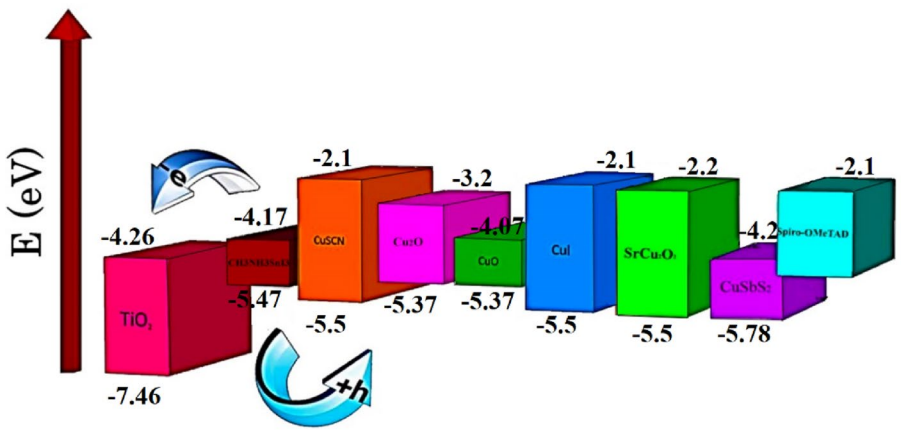

Fig. 2 Energy diagram, band edges, HOMO and LUMO levels for regular n-i-p-based PSCs [27, 47–61]

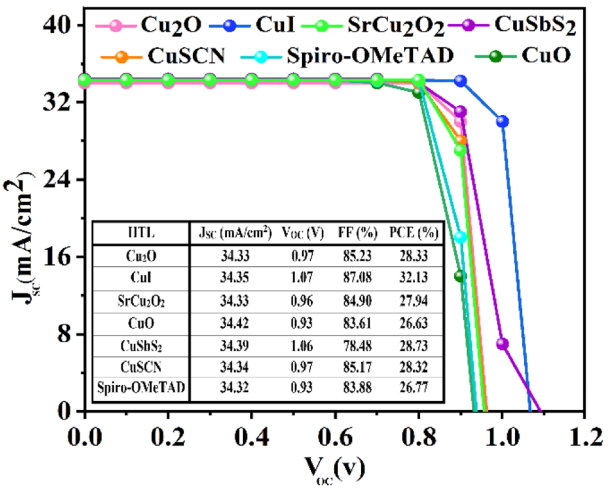

HTL	J_{SC} (mA/cm^2)	V_{OC} (V)	FF (%)	PCE (%)
Cu_2O	34.33	0.97	85.23	28.33
CuI	34.35	1.07	87.08	32.13
$SrCu_2O_2$	34.33	0.96	84.90	27.94
CuO	34.42	0.93	83.61	26.63
$CuSbS_2$	34.39	1.06	78.48	28.73
CuSCN	34.34	0.97	85.17	28.32
Spiro-OMeTAD	34.32	0.93	83.88	26.77

Fig. 3 Variation in the current–voltage curve of tin-based PSC with different HTL layers

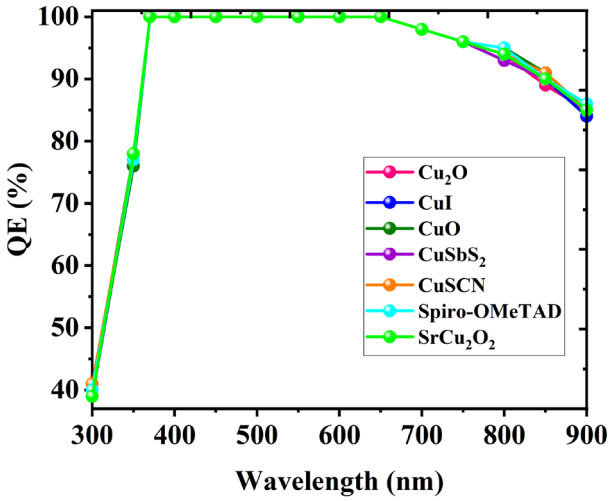

Fig. 4 The QE curves of simulated perovskite solar cell with different HTLs

blocking the extraction of the carriers, and thus decreasing FF and PCE. A significant imbalance in mobility will lead to an S-shaped *J–V* curve and very low FF. According to the *J–V* characteristics shown in Fig. 3, in comparison to other solar cells, the solar cell with CuI as HTL shows more current and less shunt resistance. CuI is an inorganic HTL that has high electron–hole mobility. Hence, the FF will increase for a solar cell with CuI as HTL. The absorption coefficient of CuI is higher compared to those of other HTLs, so it is capable of harvesting photons that were not absorbed by the perovskite layer and generating more carriers. The small band gap of CuO (1.3 eV) in comparison with the band gap of CuI (3.4 eV) might be the reason for poor performance in V_{OC} of the PSC using CuO as HTL. However, the PSC with CuSCN as HTL has the same band gap as CuI but it has a smaller FF value because of the additional electric field in the PSC [60].

3.2 Quantum efficiency (QE)

Figure 4 shows the QE curve of simulated perovskite solar cells. When the wavelength increases and becomes more than 700 nm, the efficiency of the solar cell will decrease slowly. In the range of visible light, electrons and holes are transferred perfectly. Therefore, the major reason that leads to the decreasing efficiency of the solar cells is spectral non-concurrence, the input energy of photons with the band gap of the solar cell. Photons with lower energy in comparison to band-gap cannot be absorbed by the solar cell and then the excess energy of these photons' changes to the kinetic energy of electron–hole pair, then change to heat. The ideal quantum efficiency of 100% for light absorption is in the range of 400–700 nm for the perovskite layer. Less absorption or recombination between TCO and TiO_2 and that between TO_2 and HTL layers leads to a decrease in the quantum efficiency in short and long wavelength regions. Because of recombination in HTL in long wavelengths with less diffusion length, the absorption QE decreases. There is a stable electric field inside the perovskite layer that in the HTL and ETL edges in the beginning and end of the diagram is limited to zero. The recombination rate in the perovskite layer is low while it is higher between TCO, TiO_2 and HTL and back contact layers than inside the perovskite absorber. The band gap of the perovskite layer is appropriate to absorb light and good band alignment of the energy levels in the visible spectral region lead to the feasible transfer of electrons and holes from the perovskite layer, but at near-IR spectral region, QE will decrease in comparison to the ideal value (~ 100%) because of the reflection and low diffusion length [61, 62].

3.3 Effect of the thickness modification of perovskite layer

The thickness of the perovskite layer is one of the important parameters in optimizing the performance of the PSC. There is an optimum absorber thickness corresponding to the best PCE. It should be optimized for the solar cell simulation of the photo-generated holes and electrons by their absorption and recombination [63]. According to an article by Hima et al., the thickness of the absorber layer has a great effect on the electrical properties, optical properties, energy characteristics, and morphology of solar cells [64]. The layer thickness of the absorber changes from 0.5 µm to 1 µm while keeping other parameters constant. As the layer thickness of the perovskite increases, the longer wavelength of illumination will produce an optimum number of

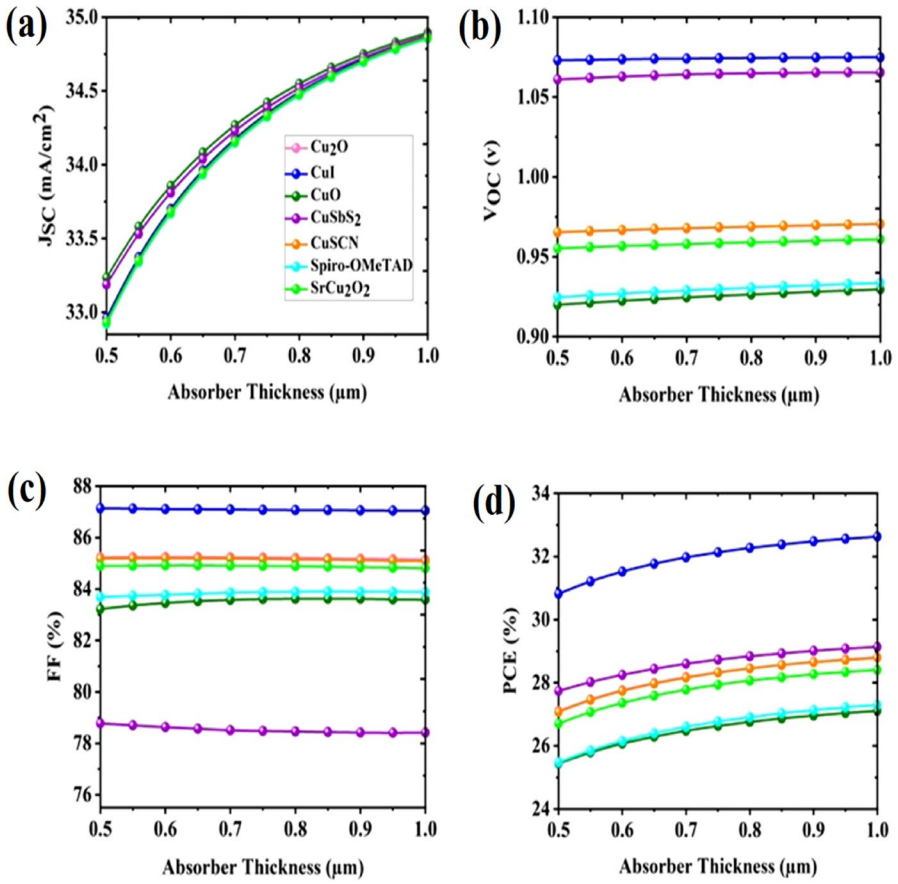

Fig. 5 Effect of thickness modification of perovskite absorber layer on photovoltaic parameters. **a** Impact of the thickness of the perovskite upon J_{SC}. **b** Impact of the thickness of the perovskite upon V_{OC}. **c** Impact of the thickness of the perovskite upon FF. **d** Impact of the thickness of the perovskite upon PCE

electron–hole pairs. Photovoltaic parameters (V_{OC}, J_{SC}, FF, and PCE) are demonstrated in Fig. 5. If the thickness of the absorber layer increases, more electron–hole pairs will be created. Thus, J_{SC} will increase and the solar cell will have more excess carrier concentrations [65]. As the thickness of the absorber layer rises, the chances of recombination also increase because the charges have to travel a long distance for diffusion [66, 67]. According to Eq. 4, the V_{OC} can be expressed as follows—

$$VOC = \frac{kT}{e} \mathrm{In}\left[\frac{J_{sc}}{J_0} + 1\right] \tag{4}$$

here, k signifies the Boltzmann constant, T signifies the operating temperature, J_{sc} signifies the short-circuit current density, J_o signifies the reverse saturation current, and e signifies the electron charge [68, 69]. The FF decreases with the increasing thickness of the adsorbent layer. This is due to the increased series resistance and recombination in the perovskite layer. There is a sharp increase in efficiency at an optimum thickness of the absorber layer which is 0.75 µm because of increasing charge carriers and more charge movement [52]. Generally, PCE depends on J_{SC}, FF, and V_{OC}. In Fig. 5, it can be seen that through more absorption of light, as the thickness of the absorber layer increases, the generation of electron–hole pair increases. Hence, the PCE increases at first because of increasing the exciton generation [65]. Recombination at the interface of layers decreases the photo-current of a solar cell and it causes a significant reduction in V_{OC} [32].

3.4 Effect of defect density (Nt) modification on photovoltaic parameters

The process of doping in the absorber layer and reducing the quality of doping levels is due to the formation of the defects and the impact of N_t upon the performance of the PSC [70]. According to the article by Akbulatov et al., defect density depends on the doping process and the quality of perovskite and the doping substance utilized and the fabrication [71]. Figure 6 demonstrates the impact of N_t of the absorber layer upon the PSC with different HTLs. In this article, we calculate the photovoltaic parameters by changing the N_t of the perovskite layer from 10^5 to 10^{12} cm^{-3}. According to the diagrams shown in Fig. 6, the low quality of the absorber layer, the increase in the defect densities and the recombination lead to a decrease in the diffusion length of charge carriers, thus decreasing the lifetime of

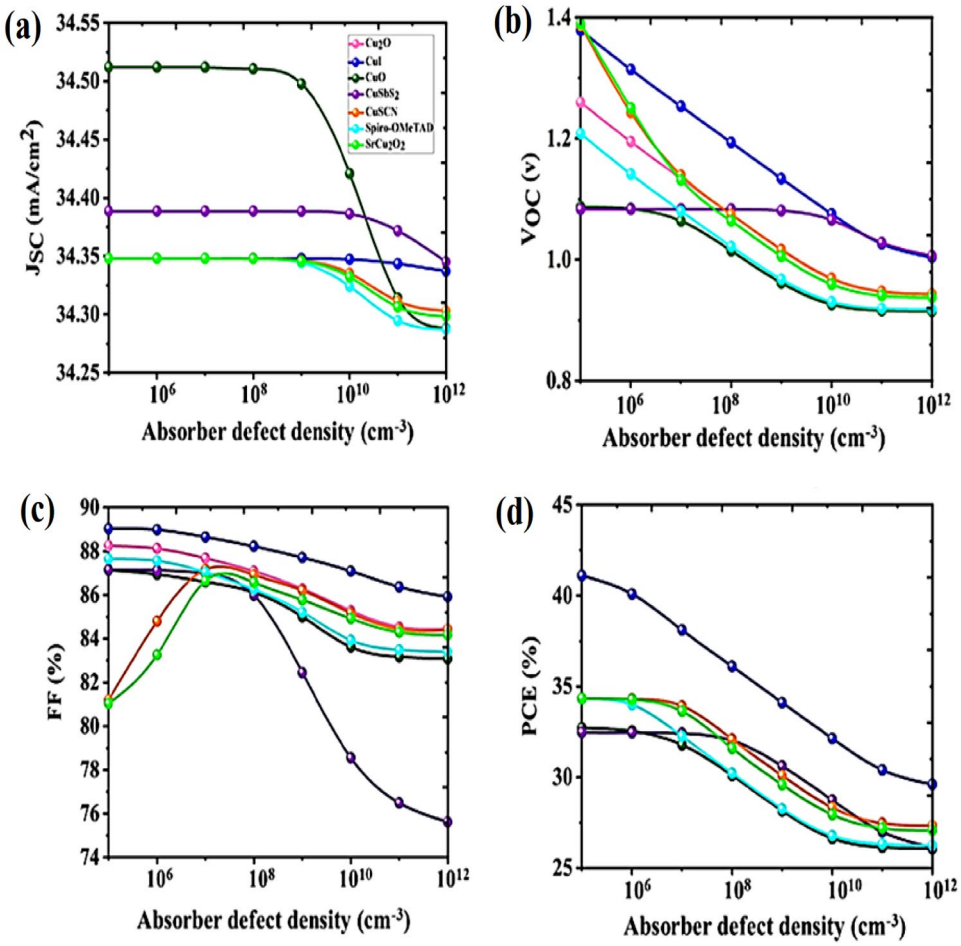

Fig. 6 Effect of defect density modification of perovskite absorber layer on photovoltaic parameters. **a** J_{SC}, **b** V_{OC}, **c** FF, and **d** PCE

carriers. As the defect densities were lower than 10^6 cm^{-2}, there was no significant variation in efficiency. Increasing carrier recombination can be described by N_t in the perovskite layer which increases the recombination process of photo-generated carriers. Hence, J_0 increases, and diffusion length, J_{SC}, and V_{OC} decrease, which leads to a decrease in the PCE [70, 71]. With increasing N_t of solar cells, carriers are difficult to move [72]. So, the band bending in the absorber layer decreases, thus decreasing the effective barrier and consequently decreasing V_{OC}, which also decreases the performance of the device [73, 74]. The availability of a larger N_t leads to an increase in the recombination rate that causes a reduction in the number of charge carriers for the CB, thereby decreasing PCE, FF, J_{SC}, and V_{OC} [18].

3.5 Effect of band gap modification on photovoltaic parameters of devices

In this section, the photovoltaic parameters will be checked in a special situation where all of the parameters of layers stay constant and the band gap only changes. In a PSC, the band gap of the perovskite layer effects on the light absorption. Hence, its changes affect the efficiency of the devices. The good band matching of HTL, perovskite layer and ETL is necessary for raising the efficiency of the solar cell. According to Eq. 5, the band gap of a semiconductor, in case the VBO becomes zero, is the least amount of energy required for the stimulation of a connective electron to a free and transfer state.

$$E_a = E_g - |\mathrm{VBO}| \tag{5}$$

The layers with low band gap energy can take the most photons in the solar spectrum, which results in a large number of excited charge carriers. Increasing interatomic spacing results in a decrease in the potential of the electron, so, the energy of the band gap decreases. Layers with wide band gaps endure more heat and radiation without losing their electrical feature. The perovskite layer has a considerable impact on *V*oc. With increasing the band gap of the perovskite layer, J_{SC} decreases due to the decrease in the optical absorption of the photons with lower energy compared to the band gap energy [75]. The V_{OC} relies upon the band gap, and because of the higher band gap, V_{OC} increases, and radiative recombination decreases.

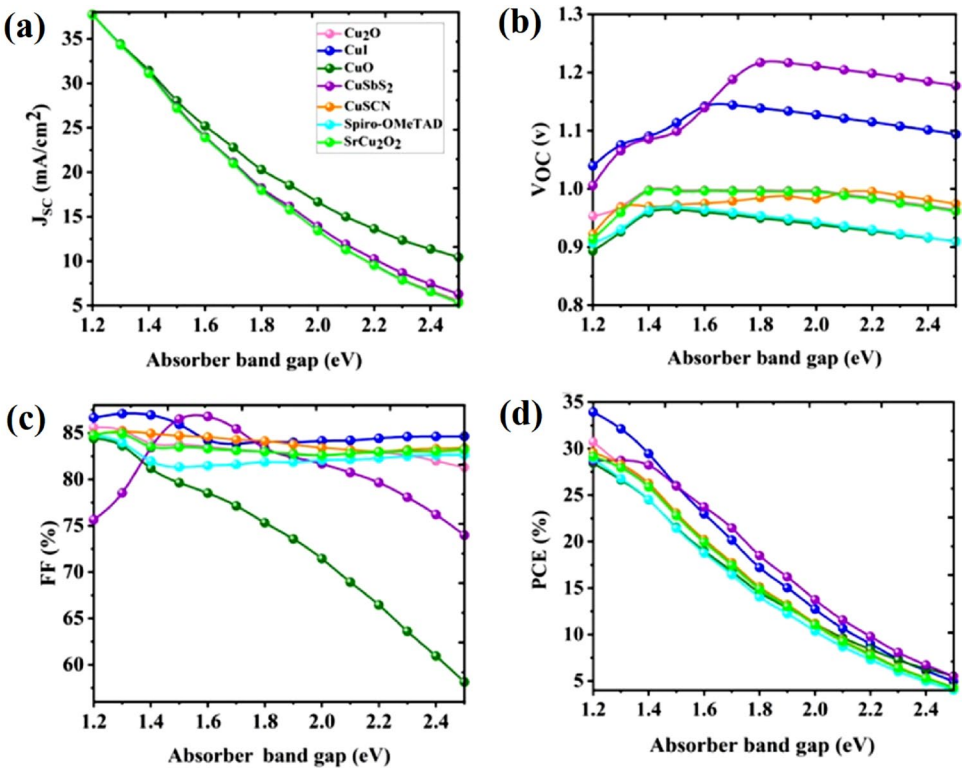

Fig. 7 Band gap modification of perovskite absorber layer. **a** Impact of the band gap of the perovskite on J_{SC}. **b** Impact of the band gap of the perovskite on V_{OC}. **c** Impact of the band gap of the perovskite on FF. **d** Impact of the band gap of the perovskite on PCE of simulated devices

According to Fig. 7b, as the band gap of the perovskite layer increases too much, recombination increases, leading to a gradual reduction in the V_{OC}, and a band gap of 1.8 eV is the optimum amount. As the band gap of the perovskite layer in the solar cell increases, the absorption of photons decreases which leads to a reduction in the efficiency of the PSC and the FF decreases because of the mismatch between the absorber layer and the HTL. According to Fig. 7, when the band gap of the perovskite increases from 1.2 to 2.5 eV, the photovoltaic parameters, such as the FF, J_{SC}, and PCE, decrease, but the V_{OC} slightly increases [76]. The best amount of band gap in a simulated solar cell is about 1.3 eV. The absorption coefficient in semiconductors is largely a function of photon energy or wavelength. In a semiconductor, light that is less than the absorption level does not have enough energy for stimulating electrons from the valence band (VB) to the conduction band (CB), so, this photon will not be absorbed [77]. Figure 7 depicts the impact of the band gap of the absorber layer upon the photovoltaic parameters. In this article, the lead-free perovskite possesses a band gap between 1.2 and 2.5 eV. In solar cells with CuO and $CuSbS_2$, as band gap and resistance increase, due to high electron affinity, FF has a sharp decrease. Electrons and holes have less mobility which leads to creating a thick interface, so, electrons and holes are absorbed to back and front contact for recombination and the FF decreases quickly.

3.6 Effect of temperature on photovoltaic parameters of simulated devices

The working temperature has a key role in the efficiency of a device. In this article, the temperature is changed from 300 to 480 K for determining the impact of working temperature on J_{SC}, V_{OC}, FF, and PCE for the optimized temperature as demonstrated in Fig. 8. In a solar cell, at the installed conditions, the temperature is higher than 300 K, but generally, the temperature of a solar cell is 300 K. Increasing the temperature of the solar cell leads to more stress and deformation in interfacial defects. So, interconnectivity between the layers decreases [78]. Increasing N_t results in a rise in recombination and a reduction in diffusion length. Because of decreasing diffusion length, series resistance increases. So, the PCE and FF of the device decrease [66, 76]. The performances of solar cells depend on temperature because different temperatures cause different band gaps. As temperature increases, because of absorbing more solar spectrum photon components, the band gap of the majority of the semiconductor layer decreases. By increasing the temperature of the solar cell, parameters, such as mobility of carriers, are affected and because of changing the resistance, stress and deformation increase, and SRH recombination increases, which results in a decrease in PCE and FF [78]. J_{SC} has slightly increased because of a reduction in the band gap energy. The band gaps, carrier density, and electron and hole mobilities of the device would be also impacted by

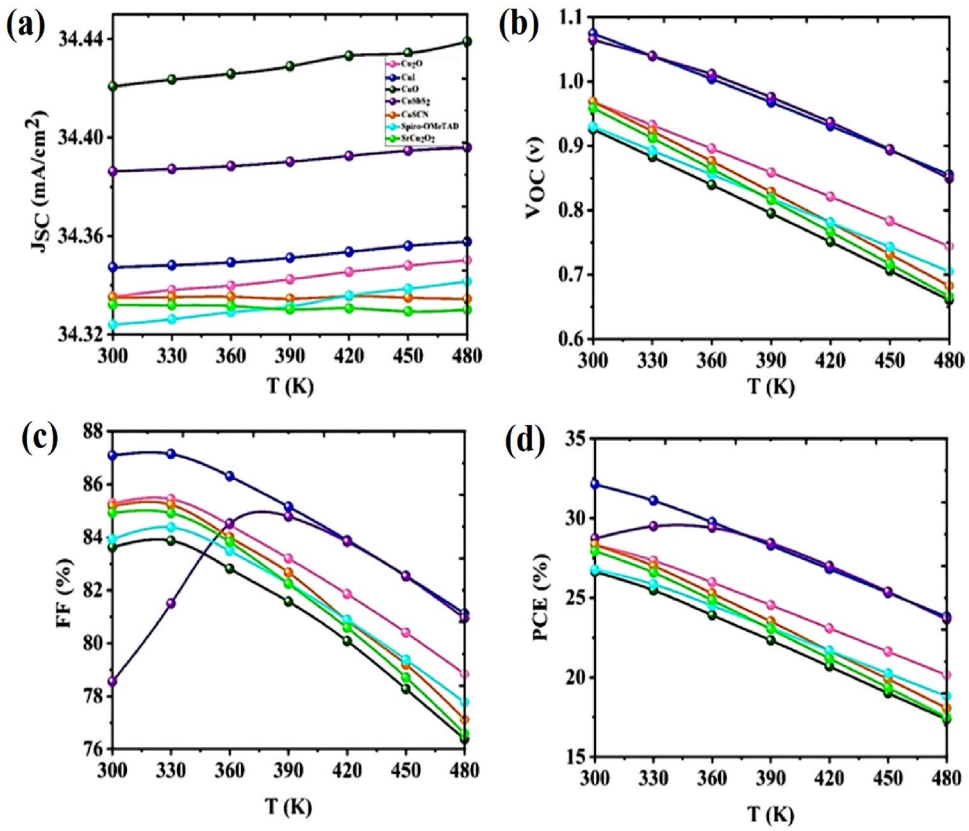

Fig. 8 Effect of temperature on photovoltaic parameters. **a** Effect of the temperature on J_{SC}. **b** Effect of the temperature on V_{OC}. **c** Effect of the temperature on FF. **d** Effect of the temperature on PCE

the change in the temperature, decreasing the efficiency of the device [79]. Decrease in the recombination by generating more charge carriers at the interface of layers causes an increase in the photo-current and J_{SC} of devices.

Decreasing V_{OC} will affect the performance of PSCs. Equation 6 shows the relation between V_{OC}, T, and E_g of perovskite in a solar cell:

$$\frac{d(V_{OC})}{dT} = \frac{(V_{OC} - \frac{E_g}{q})}{T} \tag{6}$$

where T signifies the operating temperature, E_g signifies the band gap, and q signifies the electric charge [79].

3.7 Effect of the thickness modification of HTLs

The effect of thickness of HTL on the photovoltaic performance of TPSCs was verified by varying the values of film thickness from 0.04 to 0.4 µm. The differences between efficiency of the devices as a function of HTL film thickness are shown in the Fig. 9. The photovoltaic parameters for different HTLs with varied film thicknesses are almost identical. For TPSC with CuSbS2 as HTL, due to less mobility of electrons and holes, increasing of the thickness of HTL creates a thick interfacial barrier. Therefore, electrons and holes are absorbed to back and front contacts, for this reason, FF decreases but VOC increases substantially to lead to the PCE almost constant as film thickness varied. CuI is selected as the best HTL because of great Voc and FF values. As a result, CuI-based device has the best performance due to its high carrier mobility and a proper VBO aforementioned [15].

4 Conclusions

In this study, the glass/TCO/TiO_2/$CH_3NH_3SnI_3$/Cu-based (HTL)/Au solar cell (THPSC) structure was designed and simulated by means of the SCAPS-1D software program. Cu-based substances, such as Cu-based halides, oxides, and chalcogenides, were used as HTL in PSCs in this study due to properties such as proper band alignment, low cost of production, and great hole mobility. In addition, due to the high p-type conductivity of the Cu^+-based chalcogenides, and especially halides HTLs have better performance compared to Cu-based oxides. Therefore, it affects the efficiency and other PV parameters of perovskite solar cells, which is in good alignment with experimental results [44, 80, 81]. The structure was optimized by changing the thickness, N_t, and E_g of the absorber layer, the thickness of HTL, and the temperature of the device with different Cu-based HTLs. The maximum PCE, FF, V_{OC}, and J_{SC} achieved for the solar

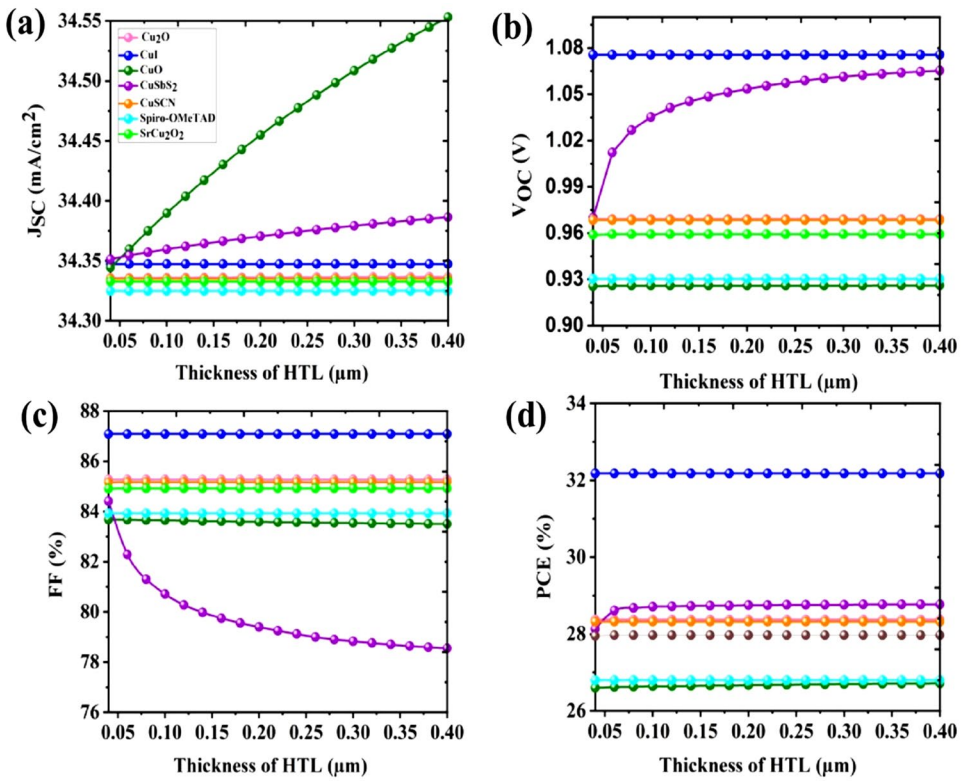

Fig. 9 Effect of thickness of HTLs on the photovoltaic parameters of simulated devices. **a** Effect of the thickness of HTL on J_{SC}. **b** Effect of the thickness of HTL on V_{OC}. **c** Effect of the thickness of HTL on FF. **d** Effect of the thickness of HTL on PCE

cell with CuI as HTL were 32.13%, 87.08%, 1.07 V, and 34.35 mA cm^{-2}, respectively. According to the results, this work can provide profound insights into designing non-toxic, cost-effective, easy processing, and high-efficiency tin halide PSCs.

Acknowledgements The authors would like to thank Prof. Marc Burgelman, the Ghent University, in Belgium, for providing the SCAPS-1D software. This work is supported by Iran National Science Foundation (INSF), Iran (Proposal No. 99014923), and National Science and Technology Council (NSTC), Taiwan (grant No. NSTC 111-2634-F-A49-007 and NSTC 111-2123-M-A49-001) and the Center for Emergent Functional Matter Science of National Yang Ming Chiao Tung University (NYCU) from The Featured Areas Research Center Program within the framework of the Higher Education Sprout Project by the Ministry of Education (MOE) in Taiwan.

Data availability All data reported in this article are available upon request to the first author or the corresponding author.

Declarations

Conflict of interest There are no conflicts of interest to declare.

References

1. J. Huang, S. Xiang, J. Yu, C.-Z. Li, Highly efficient prismatic perovskite solar cells. Energy Environ. Sci. **12**(3), 929–937 (2019)
2. K.K. Markose, M. Shaji, S. Bhatia, P.R. Nair, K.J. Saji, A. Antony, M.K. Jayaraj, Novel boron-doped p-type Cu_2O thin films as a hole-selective contact in c-Si solar cells. ACS Appl. Mater. Interfaces **12**(11), 12972–12981 (2020)
3. Y. Li, M.D. Cole, Y. Gao, T. Emrick, Z. Xu, Y. Liu, T.P. Russell, High-performance perovskite solar cells with a non-doped small molecule hole transporting layer. ACS Appl. Energy Mater. **2**(3), 1634–1641 (2019)
4. S. Imani, A. Alizadeh, M. Roudgar-Amoli, Z. Shariatinia, Inorg. Chem. Commun. **145**, 110045 (2022)
5. Y. Wang, T. Mahmoudi, Y.B. Hahn, Highly stable and efficient perovskite solar cells based on FAMA-perovskite-Cu: NiO composites with 20.7% efficiency and 80.5% fill factor. Adv. Energy Mater. **10**(27), 2000967 (2020)
6. S.M. Seyed-Talebi, I. Kazeminezhad, S. Shahbazi, E.W.G. Diau, Efficiency and stability enhancement of fully ambient air processed perovskite solar cells using TiO_2 paste with tunable pore structure. Adv. Mater. Interfaces **7**(3), 1900939 (2019)
7. S.M. Seyed-Talebi, I. Kazeminezhad, Performance improvement of fully ambient air processed perovskite solar cells in an anti-solvent process using TiO_2 hollow spheres. J. Colloid Interface Sci. **562**, 125–132 (2020)
8. Y. Wang, H. Ju, T. Mahmoudi, C. Liu, C. Zhang, S. Wu, Y. Yang, Z. Wang, J. Hu, Y. Cao, Cation-size mismatch and interface stabilization for efficient NiOx-based inverted perovskite solar cells with 21.9 % efficiency. Nano Energy **88**, 106285 (2021)
9. H.-Y. Yang, W.-Y. Rho, S.K. Lee, S.H. Kim, Y.-B. Hahn, TiO_2 nanoparticles/nanotubes for efficient light harvesting in perovskite solar cells. Nanomaterials **9**(3), 326 (2019)
10. S.M. Seyed-Talebi, J. Beheshtian, Lead-free inorganic cesium tin-germanium triiodide perovskites for photovoltaic application. Int. J. Energy Eng. **15**(6), 252–257 (2021)
11. A. Kojima, K. Teshima, Y. Shirai, T. Miyasaka, Organometal halide perovskites as visible-light sensitizers for photovoltaic cells. J. Am. Chem. Soc. **131**(17), 6050–6051 (2009)

12. H. Min, D.Y. Lee, J. Kim, G. Kim, K.S. Lee, J. Kim, M.J. Paik, Y.K. Kim, K.S. Kim, M.G. Kim, T.J. Shin, S.I. Seok, Perovskite solar cells with atomically coherent interlayers on SnO_2 electrodes. Nature **598**(7881), 444–450 (2021)
13. J.J. Yoo, G. Seo, M.R. Chua, T.G. Park, Y. Lu, F. Rotermund, Y.-K. Kim, C.S. Moon, N.J. Jeon, J.-P. Correa-Baena, Nature **590**(7847), 587 (2021)
14. S.R. Hosseini, M. Bahramgour, P.Y. Sefidi, A. Tabatabaei Mashayekh, A. Moradi, N. Delibas, MGh. Hosseini, A. Niaei, Heliyon **8**(11), e11471 (2022)
15. S. Mushtaq, S. Tahir, A. Ashfaq, R.S. Bonilla, M. Haneef, R. Saeed, W. Ahmad, N. Amin, Performance optimization of lead-free $MASnBr_3$ based perovskite solar cells by SCAPS-1D device simulation. Sol. Energy **249**, 401–413 (2023)
16. F. Izadi, A. Ghobadi, A. Gharaati, M. Minbashi, A. Hajjiah, Effect of interface defects on high efficient perovskite solar cells. Optik **227**, 166061 (2021)
17. M. Caputo, N. Cefarin, A. Radivo, N. Demitri, L. Gigli, J.R. Plaisier, M. Panighel, G. Di Santo, S. Moretti, A. Giglia, Electronic structure of $MAPbI_3$ and $MAPbCl_3$: importance of band alignment. Sci. Rep. **9**(1), 1–11 (2019)
18. I.M. De Los Santos, H.J. Cortina-Marrero, M. Ruíz-Sánchez, L. Hechavarría-Difur, F. Sánchez-Rodríguez, M. Courel, H. Hu, Optimization of $CH_3NH_3PbI_3$ perovskite solar cells: a theoretical and experimental study. Sol. Energy **199**, 198–205 (2020)
19. D. Liu, Q. Li, J. Hu, H. Jing, K. Wu, Predicted photovoltaic performance of lead-based hybrid perovskites under the influence of a mixed-cation approach: theoretical insights. J. Mater. Chem. C. **7**(2), 371–379 (2019)
20. M. Green, E.D. Dunlop, J. Hohl-Ebinger, M. Yoshita, N. Kopidakis, X. Ho, Solar cell efficiency tables (Version 55). Prog. Photovoltaics Res. Appl. **28**(1), 3–15 (2020)
21. W. Ke, M.G. Kanatzidis, Prospects for low-toxicity lead-free perovskite solar cells. Nat. commun. **10**(1), 1–4 (2019)
22. X. Jiang, Z. Zang, Y. Zhou, H. Li, Q. Wei, Z. Ning, Tin halide perovskite solar cells: an emerging thin-film photovoltaic technology. Acc. Mater. Rea. **2**(4), 210–219 (2021)
23. K. Nishimura, M.A. Kamarudin, D. Hirotani, K. Hamada, Q. Shen, S. Iikubo, T. Minemoto, K. Yoshino, S. Hayase, Lead-free tin-halide perovskite solar cells with 13% efficiency. Nano Energy **74**, 104858 (2020)
24. W. Ke, C.C. Stoumpos, M.G. Kanatzidis, "Unleaded" perovskites: status quo and future prospects of tin-based perovskite solar cells. Adv. Mater. **31**(47), 1803230 (2019)
25. M.A. Kamarudin, D. Hirotani, Z. Wang, K. Hamada, K. Nishimura, Q. Shen, T. Toyoda, S. Iikubo, T. Minemoto, K. Yoshino, Suppression of charge carrier recombination in lead-free tin halide perovskite via Lewis base post-treatment. J. Phys. Chem. Lett. **10**(17), 5277–5283 (2019)
26. E. Jokar, C.H. Chien, C.M. Tsai, A. Fathi, E.W.-G. Diau, Robust tin-based perovskite solar cells with hybrid organic cations to attain efficiency approaching 10%. Adv. Mater. **31**(2), 1804835 (2019)
27. N.K. Noel, S.D. Stranks, A. Abate, C. Wehrenfennig, S. Guarnera, A.-A. Haghighirad, A. Sadhanala, G.E. Eperon, S.K. Pathak, M.B. Johnston, Lead-free organic–inorganic tin halide perovskites for photovoltaic applications. Energy Environ. Sci. **7**(9), 3061–3068 (2014)
28. S. Bhattarai, T. Das, Optimization of the perovskite solar cell design to achieve a highly improved efficiency. Optic. Mater. **111**, 110661 (2021)
29. E. Karimi, S.M.B. Ghorashi, The effect of SnO_2 and ZnO on the performance of perovskite solar cells. J. Electron. Mater. **49**(1), 364–376 (2020)
30. G.M. Arumugam, S.K. Karunakaran, C. Liu, C. Zhang, F. Guo, S. Wu, Y. Mai, Inorganic hole transport layers in inverted perovskite solar cells: A review. Nano Select. **2**(6), 1081–1116 (2021)
31. D. Sharma, R. Mehra, B. Raj, Optimization of tin based perovskite solar cell employing $CuSbS_2$ as HTL: A numerical simulation approach. Optic Mater **134 A**, 113060 (2022)
32. F. Baig, *Numerical analysis for efficiency enhancement of thin film solar cells* (Universitat Politècnica de València, 2019)
33. R. Singh, P.K. Singh, B. Bhattacharya, H.-W. Rhee, Review of current progress in inorganic hole-transport materials for perovskite solar cells. Appl. Mater. Today **14**, 175 (2019)
34. Z. Yu, L. Sun, Inorganic hole-transporting materials for perovskite solar cells. Small Methods **2**(2), 1700280 (2018)
35. A. Kumar, S. Singh, A. Yadav, Recent development in copper based hole transport materials for emerging inverted perovskite solar cells. Mater. Sci. Eng. **1116**, 012066 (2021)
36. J.S. Shaikh, N.S. Shaikh, Y.K. Mishra, P. Kanjanaboos, P.M. Shewale, S. Sabale, S. Praserthdam, C.D. Lokhande, Low-cost Cu-based inorganic hole transporting materials in perovskite solar cells: Recent progress and state-of-art developments. Mater. Today Chem. **20**, 100427 (2021)
37. M. Shasti, A. Mortezaali, (2019), Numerical study of Cu_2O, $SrCu_2O_2$, and $CuAlO_2$ as hole-transport materials for application in perovskite solar cells. Phys. Status Solidi A **216**, 1900337 (2019)
38. S. Sharma, A.K. Sharma, Improved cuprous iodide and tin halide based perovskite solar cell design for better fill factor and power conversion efficiency. Mater. Today: Proc. **28**(3), 1955–1961 (2020)
39. J.T. Matondo, D.M. Maurice, Q. Chen, L. Bai, M. Guli, Inorganic copper-based hole transport materials for perovskite photovoltaics: challenges in normally structured cells, advances in photovoltaic performance and device stability. Sol. Energy. Mater. Sol. Cells. **224**, 111011 (2021)
40. T. Ye, X. Sun, X. Zhang, S. Hao, Recent advances of Cu-based hole transport materials and their interface engineering concerning different processing methods in perovskite solar cells. J. Energy Chem. **62**, 459–476 (2021)
41. Z. Omarova, D. Yerezhep, A. Aldiyarov, N. Tokmoldin, In silico investigation of the impact of hole-transport layers on the performance of $CH_3NH_3SnI_3$ perovskite photovoltaic cells. Crystals **12**(5), 699 (2022)
42. A.P. Shyma, R. Sellappan, Computational probing of tin-based lead-free perovskite solar cells: effects of absorber parameters and various electron transport layer materials on device performance. Materials **15**(21), 7859 (2022)
43. A. Niemegeers, M. Burgelman, S. Degrave, J. Verschraegen, K. Decock, *SCAPS (Version: 3.3. 07) manual November 7, 2018* (University of Gent, Gent, 2020)
44. J. Ge, C.R. Grice, Y. Yan, Cu-based quaternary chalcogenide Cu_2BaSnS_4 thin films acting as hole transport layers in inverted perovskite $CH_3NH_3PbI_3$ solar cells. J. Mater. Chem. A **5**(6), 2920–2928 (2017)
45. T. Garmim, N. Benaissa, L. Soussi, R. Mghaiouini, C. El Ghaouti, Z. El Jouad, A. Louardi, B. Hartiti, M. Monkade, Effect of alternative buffer layers for SnS based solar cells: numerical analysis using SCAPS-1D. Mater. Today Proc. **66**, 146–150 (2022)
46. Y. Raoui, H. Ez-Zahraouy, N. Tahiri, O. El Bounagui, S. Ahmad, S. Kazim, Performance analysis of $MAPbI_3$ based perovskite solar cells employing diverse charge selective contacts: simulation study. Sol. Energy. **193**, 948–955 (2019)
47. F. Hao, C. Stoumpos, D. Cao, R. Chang, M. Kanatzidis, Nat. Photonics **8**(489), 2014 (2014)
48. V. Pfeifer, P. Erhart, S. Li, K. Rachut, J. Morasch, J. Brötz, P. Reckers, T. Mayer, S. Rühle, A. Zaban, Energy band alignment

between anatase and rutile TiO_2. J. Phys. Chem. Lett. **4**(23), 4182–4187 (2013)
49. M. Hossain, F. Alharbi, Recent advances in alternative material photovoltaics. Mater. Technol. **28**(1–2), 88–97 (2013)
50. T. Zhao, W. Shi, J. Xi, D. Wang, Z. Shuai, Intrinsic and extrinsic charge transport in $CH_3NH_3PbI_3$ perovskites predicted from first-principles. Sci. Rep. **6**(1), 1–9 (2016)
51. P. Umari, E. Mosconi, F. De Angelis, Relativistic GW calculations on $CH_3NH_3PbI_3$ and $CH_3NH_3SnI_3$ perovskites for solar cell applications. Sci. Rep. **4**(1), 1–7 (2014)
52. R. Sharma, R. Mehra, Perovskite solar cell design using Tin Halide and cuprous thiocyanate for enhanced efficiency. Int. J. Eng. Adv. Technol. **8**(16), 2817–2825 (2019)
53. A.B. Coulibaly, S.O. Oyedele, B. Aka, Comparative study of lead-free perovskite solar cells using different hole transporter materials. Mod. Numer. Simul. Mater. Sci. **9**(4), 97–107 (2019)
54. S. Ahmed, F. Jannat, M.A.K. Khan, M. Abdul Alim, Numerical development of eco-friendly Cs2TiBr 6 based perovskite solar cell with all-inorganic charge transport materials via SCAPS-1D. Optik **225**, 165765 (2021)
55. D. Jalalian, A. Ghadimi, A. Kiani Sarkaleh, Investigation of the effect of band offset and mobility of organic/inorganic HTM layers on the performance of perovskite solar cells. J. Optoelectron. Nanostruct. **5**(2), 65–78 (2020)
56. M. Shasti, A. Mortezaali, Numerical study of Cu2O, SrCu2O2, and CuAlO2 as hole-transport materials for application in perovskite solar cells. Phys. Status Solidi (a) **216**(18), 1900337 (2019)
57. C. Devi, R. Mehra, Device simulation of lead-free $MASnI_3$ solar cell with $CuSbS_2$ (copper antimony sulfide). J. Mater. Sci. **54**(7), 5615–5624 (2019)
58. G. Casas, M.Á. Cappelletti, A.P. Cedola, B.M. Soucase, E.P. yBlancá, Analysis of the power conversion efficiency of perovskite solar cells with different materials as hole-transport layer by numerical simulations. Superlattices. Microstruct. **107**, 136–143 (2017)
59. J. Even, L. Pedesseau, O. Durand, M. Modreanu, G. Huyberechts, B. Servet, O. Chaix-Pluchery, Vibrational properties of $SrCu_2O_2$ studied via density functional theory calculations and compared to Raman and infrared spectroscopy measurements. Thin Solid Films **541**, 113–116 (2013)
60. A.O. Maka, T.S. O'Donovan, Effect of thermal load on performance parameters of solar concentrating photovoltaic: high-efficiency solar cells. Energy. Built Environ. **3**(2), 201–209 (2022)
61. R.I. Rabady, Optimized multi-junction photovoltaic solar cells for terrestrial applications. Sol. Energy **106**, 72–81 (2014)
62. Y.P. Varshni, Temperature dependence of the energy gap in semiconductors. Physica **34**(1), 149–154 (1967)
63. A. Rozhko, V. Petrov, A. Sayenko, Study of the effect of the thickness of the photosensitive layer of perovskite on its efficiency using SCAPS-1D software, in *IOP conference series materials science and engineering*. (IOP Publishing, 2021), p.012032
64. A. Hima, N. Lakhdar, B. Benhaoua, A. Saadoune, I. Kemerchou, F. Rogti, An optimized perovskite solar cell designs for high conversion efficiency. Superlatt. Microstruct. **129**, 240–246 (2019)
65. Z.-Q. Li, M. Ni, X.-D. Feng, Simulation of the Sb_2Se_3 solar cell with a hole transport layer. Mater. Res. Express **7**(1), 016416 (2020)
66. A. Slami, M. Bouchaour, L. Merad, Comparative study of modelling of Perovskite solar cell with different HTM layers. Int. J. Mater **7**, 2313–10555 (2020)
67. Y. Gan, X. Bi, Y. Liu, B. Qin, Q. Li, Q. Jiang, P. Mo, Numerical investigation energy conversion performance of tin-based perovskite solar cells using cell capacitance simulator. Energies **13**(22), 5907 (2020)
68. M.T. Islam, M.R. Jani, S.M. Al Amin, M.S.U. Sami, K.M. Shorowordi, M.I. Hossain, M. Devgun, S. Chowdhury, S. Banerje, S. Ahmed, Numerical simulation studies of a fully inorganic Cs2AgBiBr 6 perovskite solar device. Optic. Mater. **105**, 109957 (2020)
69. I. Alam, M.A. Ashraf, Effect of different device parameters on tin-based perovskite solar cell coupled with In_2S_3 electron transport layer and CuSCN and Spiro-OMeTAD alternative hole transport layers for high-efficiency performance. Energy Sour. Part A **45**, 1–17 (2020)
70. B.A. Al-Asbahi, S.M. Qaid, M. Hezam, I. Bedja, H.M. Ghaithan, A.S. Aldwayyan, Effect of deposition method on the structural and optical properties of $CH_3NH_3PbI_3$ perovskite thin films. Optic. Mater. **103**, 109836 (2020)
71. A.F. Akbulatov, L.A. Frolova, S.A. Tsarev, I. Zhidkov, S.Y. Luchkin, E.Z. Kurmaev, K.J. Stevenson, S.M. Aldoshin, P.A. Troshin, Film deposition techniques impact the defect density and photostability of $MAPbI_3$ Perovskite films. J. Phys. Chem. C. **124**(39), 21378–21385 (2020)
72. M. Samiul Islam, K. Sobayel, A. Al-Kahtani, M. Islam, G. Muhammad, N. Amin, M. Shahiduzzaman, M. Akhtaruzzaman, Defect study and modelling of SnX_3-based perovskite solar cells with SCAPS-1D. Nanomaterials **11**(5), 1218 (2021)
73. K. Sobayel, M. Akhtaruzzaman, K. Rahman, M. Ferdaous, Z.A. Al-Mutairi, H.F. Alharbi, N.H. Alharthi, M.R. Karim, S. Hasmady, N. Amin, A comprehensive defect study of tungsten disulfide (WS_2) as electron transport layer in perovskite solar cells by numerical simulation. Results Phys. **12**, 1097–1103 (2019)
74. N. Singh, A. Agarwal, M. Agarwal, Numerical simulation of highly efficient lead-free all-perovskite tandem solar cell. Sol. Energy. **208**, 399–410 (2020)
75. J.L. Prasanna, E. Goel, A. Kumar, A. Laref, C. Santhosh, P. Ranjan, A. Kumar, Bandgap graded perovskite solar cell for above 30% efficiency. Optik **269**, 169891 (2022)
76. U. Mandadapu, S.V. Vedanayakam, K. Thyagarajan, M.R. Reddy, B. Babu, Design and simulation of high efficiency tin halide perovskite solar cell. Int. J. Renew. Energy Res. **7**(4), 1603–1612 (2017)
77. S.M. Sze, Y. Li, K.K. Ng, *Physics of semiconductor devices* (John wiley & sons, 2021)
78. S. Zandi, P. Saxena, N.E. Gorji, Numerical simulation of heat distribution in RGO-contacted perovskite solar cells using COMSOL. Sol. Energy. **197**, 105–110 (2020)
79. N. Devi, K.A. Parrey, A. Aziz, S. Datta, Numerical simulations of perovskite thin-film solar cells using a CdS hole blocking layer. J. Vacuum Sci. Technol. B Nanotechnol. Microelect **36**(4), 04G105 (2018)
80. Y. Ishigaki, K. Shimomura, K. Asai, T. Shimajiri, T. Akutagawa, T. Fukushima, T. Suzuki, Chalcogen Bond versus halogen bond: changing contributions in determining the crystal packing of Dihalobenzo chalcogenadiazoles. Bull. Chem. Soc. Jpn. **95**(3), 522–531 (2022)
81. R. Okumura, T. Oku, A. Suzuki, M. Okita, S. Fukunishi, T. Tachikawa, T. Hasegawa, Effects of adding alkali metals and organic cations to Cu-based perovskite solar cells. Appl. Sci. **12**(3), 1710 (2022)